Available online at www.sciencedirect.com

ScienceDirect

Energy Procedia 81 (2015) 977 – 986

Energy Procedia

69th Conference of the Italian Thermal Engineering Association, ATI 2014

About Multi-Resolution Techniques for Large Eddy Simulation of Reactive Multi-Phase Flows

G. Rossi*, B. Favini[a], E. Giacomazzi, F. R. Picchia, N. M. S. Arcidiacono[b]

[a]*Mechanical and Aerospace Enginnering Department, Sapienza University of Rome, Via Eudossiana 18, 00184 Rome*
[b]*Technical Unit for Advanced Technologies for Energy and Industry, ENEA, via Anguillarese 301, 00123 S. M. Galeria, Rome*

Abstract

A numerical technique for mesh refinement in the HeaRT (Heat Release and Transfer) numerical code is presented. In the CFD framework, Large Eddy Simulation (LES) approach is gaining in importance as a tool for simulating turbulent combustion processes, also if this approach has an high computational cost due to the complexity of the turbulent modeling and the high number of grid points necessary to obtain a good numerical solution. In particular, when a numerical simulation of a big domain is performed with a structured grid, the number of grid points can increase so much that the simulation becomes impossible: this problem can be overcomed with a mesh refinement technique. Mesh refinement technique developed for HeaRT numerical code (a staggered finite difference code) is based on an high order reconstruction of the variables at the grid interfaces by means of a least square quasi-eno interpolation: numerical code is written in modern Fortran (2003 standard of newer) and is parallelized using domain decomposition and message passing interface (MPI) standard.

Peer-review under responsibility of the Scientific Committee of ATI 2014
Keywords: LES, Fortran, mesh-refinement, multiphase

1. Introduction

Turbulent flow field is very common in energy production burners: some particular phenomena that occur in this plants are heavily conditioned by interaction between turbulent structures and burner walls, injectors, or the flame front.

In particular, to avoid combustion instabilities and blow out phenomena, swirlers and bluff bodies are widely used: in this way oxidizer and fuel (or mixture) flows have all the three components of velocity vector different from zero; for this reason is obvious that turbulence of the flow field has a fundamental role in energy production burners behaviour.

Usually in energy production burners, inlet flow (premiscelated or not) in combustion chamber has high velocity and injectors have very little dimensions: so a numerical simulation based on DNS (Direct Numerical Simulation)

* Corresponding author. Tel.: +39-06-30484690.
E-mail address: giacomo.rossi@uniroma1.it

Peer-review under responsibility of the Scientific Committee of ATI 2014
doi:10.1016/j.egypro.2015.12.156

approach is impossible; a numerical simulation based on RANS (Reynolds Averaged Navier-Stokes) approach is very difficult to obtain because of the complexity to obtain a turbulence model suitable to the solution of such flow field (thermal and chemical non equilibrium, with complex geometries).

So numerical simulation based on LES (Large Eddy Simulation) approach is growing in importance because when a sufficient portion of the energy spectrum is resolved, is possible to obtain very good numerical results, also if computational cost is anyway high (but no so high as in DNS approach), because grid cell dimension is necessarily little to obtain a good solution of significant turbulent scales.

Modern energy production burners have usually big dimensions and a cylindrical shape, with multi-phase flow: also if a LES numerical simulation for such burners is the ideal choice, there are some problems to obtain a good numerical result: in particular, is necessary a large number of grid points to guarantee sufficient resolution to solve little turbulent scales next to the little injectors; multi-phase flow is another constraint on the dimension of grid cell, because solid particles or droplets cannot be bigger than a single grid cell.

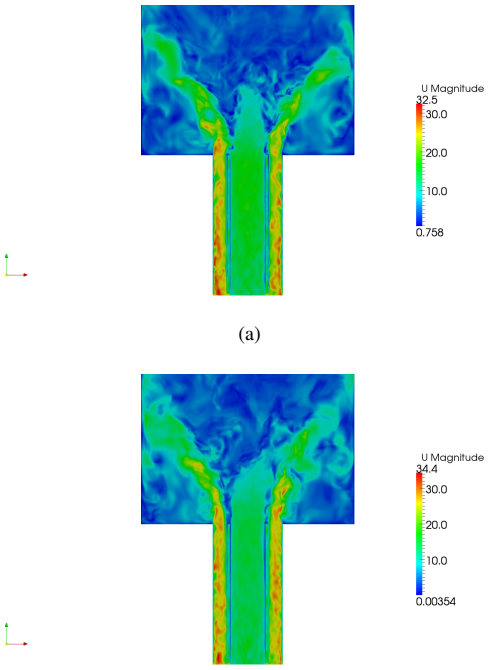

Fig. 1: Velocity Magnitude [m/s]

For example, in figure 1 are illustrated numerical results of a LES simulation of a particle laden flow, based on Sommerfeld and Qiu experiment: the injection system is composed of a cylindrical duct and of an annular duct coaxial to the first one. Air and glass particles (diameter between $20\mu m$ and $80\mu m$) flow through the cylindrical duct to the test cylindrical chamber, while from the annular duct a swirled air flow is introduced in the test section.

Also if the numerical solution globally has a good agreement with experimental data, and the presence of many small flow structures is captured as the position of the stagnation point, typical for swirled combustors, in proximity of the test chamber inlet zone radial velocity component and its RMS are not well predicted (figure 2): this can be dued to the poor resolution adopted in front of the bluff body separating the inner and the outer duct; in fact, since $\Delta z = 3mm$, only 3 grid points are present before the plane where the measures are taken and therefore it will not be possible to reconstruct smaller structures in that zone.

Total number of grid points for this numerical simulation (more than 4 millions) makes impossible to decrease Δz minimum and increase resolution, also because of the use of structured grids.

So a mesh refinement technique is mandatory to obtain a good numerical solution (with a relatively low computational cost) based on LES approach: numerical grid is divided in several structured grids with different spatial resolution: next to fuel and oxidizer injectors, where turbulent scales have a very little characteristic dimension, grid cells have very little dimensions, while in the outlet zone of the burner or the test section, where flow velocities and flow turbulence are low, grid cells have bigger dimensions.

2. HeaRT Numerical Code

HeaRT (Heat Release and Turbulence) numerical code, developed by ENEA in collaboration with Mechanical and Aerospace Engineering Department of Sapienza University of Rome, is an unsteady numerical solver for turbulent

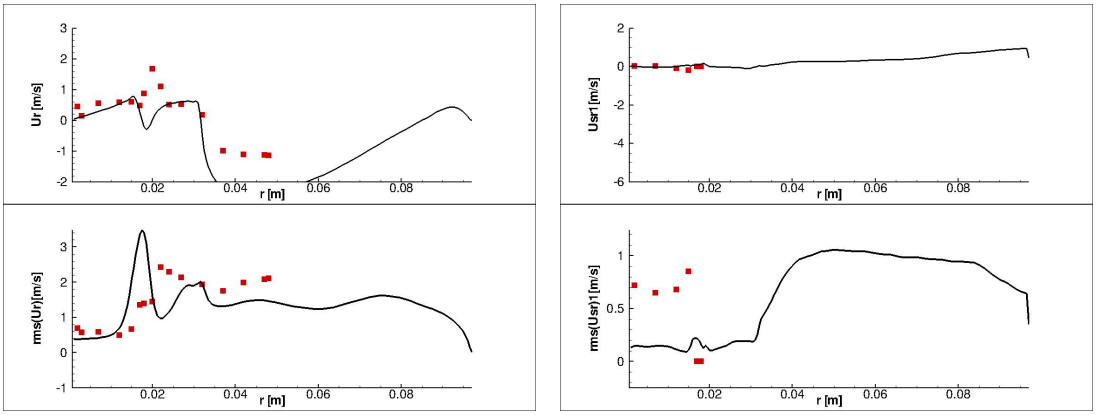

(a) (b)

Fig. 2: Velocity Component [m/s] and RMS along r direction

reacting and non reacting flows, at low Mach number, in three-dimensional cartesian and cylindrical geometries, discretized by the means of structured grids. Navier-Stokes equation are implemented in the compressible formulation, in order to highlight wave propagation phenomena that are very important for combustion instability analysis.

Mathematical model is developed for a N-species reacting Newtonian flow; heat transfer is limited to the condution and radiation contibutions, and to the enthalpic flow dued to chemical diffusion; the mass flow for a single chemical specie is limited to the diffusion contribution, modelled by the means of Hirscfelder-Curtiss law.

Numerical code is written in modern Fortran 95 and is parallelized using domain decomposition and message passing interface (MPI) standard.

2.1. Governing Equations for Gas Phase

Gas combustion is governed by a set of equation, written in differential form:

- Conservation of Mass

$$\frac{\partial \rho}{\partial t} + \nabla \cdot (\rho \mathbf{u}) = 0 \tag{1}$$

- Conservation of Linear Momentum

$$\frac{\partial \rho \mathbf{u}}{\partial t} + \nabla \cdot (\rho \mathbf{u}\mathbf{u}) = \nabla \cdot \underline{\mathbf{S}} + \rho \sum_{i=1}^{N_s} Y_i \mathbf{f_i} \tag{2}$$

- Conservation of Energy (Internal and Kinetic)

$$\frac{\partial \rho (\mathcal{E} + \mathcal{K})}{\partial t} + \nabla \cdot [\rho \mathbf{u} (\mathcal{E} + \mathcal{K})] = \nabla \cdot (\underline{\mathbf{S}}\mathbf{u}) - \nabla \cdot \mathbf{q} + \rho \sum_{i=1}^{N_s} Y_i \mathbf{f_i} \cdot (\mathbf{u} + \mathbf{V_i}) \tag{3}$$

- Conservation of Mass Fraction (for an i^{th}-specie)

$$\frac{\partial \rho Y_i}{\partial t} + \nabla \cdot (\rho \mathbf{u} Y_i) = -\nabla \cdot \mathbf{J_i} + \rho \omega_i \tag{4}$$

- Equation of State

$$p = \rho \sum_{i=1}^{N_s} \frac{Y_i}{W_i} \mathcal{R}_u T \tag{5}$$

2.2. Governing Equations for Dispersed Phase

Governing equations for dispersed phase are obtained from the evolution of the probability density function (that gives the number of particles that at time instant t are in the volume $\mathbf{x} + \mathbf{dx}$), with a velocity $\mathbf{V_p}$ within the range $\mathbf{c}_p + \mathbf{dc}_p$, temperature ϑ_p within the range $\zeta_p + d\zeta_p$ and diameter δ_p within the range $\beta_p + d\beta_p$), described by the Maxwell-Boltzmann equation:

$$\frac{\partial f_p}{\partial t} + \frac{\partial c_{p,j} f_p}{\partial x_j} + \frac{\partial \dot{c}_{p,j} f_p}{\partial c_{p,j}} + \frac{\partial \dot{\beta}_p f_p}{\partial \beta_p} + \frac{\partial \dot{\zeta}_p f_p}{\partial \zeta_p} = \left(\frac{\delta f_p}{\delta t}\right)_{coll} \tag{6}$$

After some maths, the following equations are obtained:

$$\frac{\partial}{\partial t} \int_{\mathcal{V}} r\mathbf{U} d\mathcal{V} = -\oint_{\partial \mathcal{V}} r\underline{\mathbf{F}} \cdot \hat{n} dS + \oint_{\partial \mathcal{V}} r\underline{\mathbf{G}} \cdot \hat{n} dS + \int_{\mathcal{V}} \mathbf{H} d\mathcal{V} \tag{7}$$

where $d\mathcal{V} = dr dz d\vartheta$ and

$$\mathbf{U} = \begin{Bmatrix} n_p \\ \alpha_p \rho_p \\ \alpha_p \rho_p u_{p,r} \\ \alpha_p \rho_p u_{p,\vartheta} \\ \alpha_p \rho_p u_{p,z} \\ \alpha_p \rho_p H_p \\ \alpha_p \rho_p \delta\theta_p \end{Bmatrix} \qquad \mathbf{P} = \begin{Bmatrix} 0 \\ 0 \\ \mathbb{P} \\ \mathbb{P} \\ \mathbb{P} \\ 0 \\ \delta\mathbf{Q}_j \end{Bmatrix} \qquad \mathbf{F}_{ij} = \left(U_i u_{p,j} - P_i\right) \mathbf{e}_j \tag{8}$$

$$\mathbb{P} = \alpha_p \rho_p \left[-\frac{2}{3} \tau_p \delta\theta_p + \frac{\tau_p}{3} \left(\frac{\partial \delta\theta_p}{\partial t} + u_{p,r} \frac{\delta\theta_p}{\partial r} + \frac{u_{p,\vartheta}}{r} \frac{\partial \delta\theta_p}{\partial \vartheta} + u_{p,z} \frac{\partial \delta\theta_p}{\partial z} \right) \right] \tag{9}$$

$$\delta\mathbf{Q} = \left[\frac{5}{3} \tau_p \delta\theta_p \nabla\left(\alpha_p \rho_p \delta\theta_p\right) - \frac{5}{6} \tau_p \left(\delta\theta_p\right)^2 \nabla\left(\alpha_p \rho_p\right) + \frac{5}{6} \tau_p \alpha_p \rho_p \delta\theta_p \left(\frac{D\mathbf{u}_p}{Dt} - \mathbf{a} \right) \right] \tag{10}$$

$$\underline{\mathbf{E}}_\mathbf{p} = \frac{1}{2} \left[\nabla\mathbf{u} + (\nabla\mathbf{u})^T \right] \tag{11}$$

$$\mathbf{G}_{ij} = \begin{Bmatrix} 0 \\ 0 \\ \alpha_p \rho_p \frac{\tau_p \delta\theta_p}{3} E_{rj} \mathbf{e}_j \\ \alpha_p \rho_p \frac{\tau_p \delta\theta_p}{3} E_{\vartheta j} \mathbf{e}_j \\ \alpha_p \rho_p \frac{\tau_p \delta\theta_p}{3} E_{zj} \mathbf{e}_j \\ 0 \\ 0 \end{Bmatrix} \tag{12}$$

$$\mathbf{H} = \begin{Bmatrix} 0 \\ 0 \\ \alpha_p \rho_p \left[u_{p,\vartheta}^2 - \frac{2}{3} \tau_p \delta\theta_p \left(\frac{\partial u_{p,\vartheta}}{\partial \vartheta} + u_{p,r} \right) + r \left(\frac{u_{f,r} - u_{p,r}}{\tau_p} + g_r \right) \right] \\ \alpha_p \rho_p \left[-u_{p,\vartheta} u_{p,r} - \frac{\tau_p}{3} \delta\theta_p \left(\frac{\partial u_{p,\vartheta}}{\partial r} + \frac{1}{r} \frac{\partial u_{p,r}}{\partial \vartheta} - \frac{u_{p,\vartheta}}{r} \right) + r \left(\frac{u_{f,\vartheta} - u_{p,\vartheta}}{\tau_p} + g_\vartheta \right) \right] \\ \alpha_p \rho_p \left[+r \left(\frac{u_{f,z} - u_{p,z}}{\tau_p} + g_z \right) \right] \\ 0 \\ -\frac{2r\alpha_p \rho_p}{\tau_p} \delta\theta_p + \Phi_p \end{Bmatrix} \tag{13}$$

$$\mathbf{e}_r = \mathbf{i}_r \quad \mathbf{e}_\vartheta = \frac{\mathbf{i}_\vartheta}{r} \quad \mathbf{e}_z = \mathbf{i}_z \tag{14}$$

with $\mathbf{i}_j$ is the unity module vector in the j^{th} direction.

2.3. Numerical Model

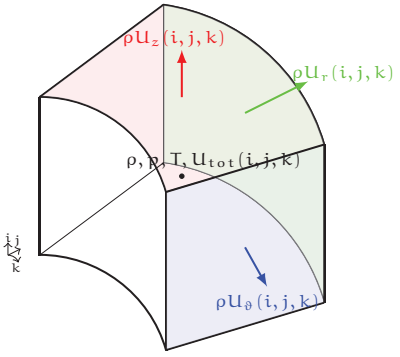

Fig. 3: Variable Position in a Cell

Governing equations are solved, in HeaRT numerical code, with a second order centered staggered numerical scheme: scalars (density, temperature, pressure, total energy, kinetic turbulent energy and mass fractions) are set in the cell center, while the three mass fluxes are set in the positive faces of the cell (see figure 3).

Viscous stresses are set in the cell center and in the edges.

This discretization technique leads to a bigger precision and a better discretization of equation 1, that doesn't need any interpolation. Because of this particular variables location, in a cylindrical geometry the axis is treated as a boundary condition and variable values are calculated by the means of a linear extrapolation from neighboring nodes.

Dispersed phase equations are numerically solved on the same computational grid used for scalar variables, by means of a finite volume technique (Godunov's scheme) with an ENO type scheme for Riemann problem solution at the cell interfaces.

For inlet and outlet boundary conditions, NSCBC (Navier-Stokes Characteristic Boundary Conditions) is adopted: in this way Navier-Stokes equation on the boundaries are solved with in terms of acustical waves amplitude on the boundary itself; derivatives orthogonal to the boundary are calculated by a first order non-centered numerical scheme: this order change ensures a global accuracy that is of the same order of the numerical scheme adopted for the numerical integration of Navier-Stokes equation in the internal flow field.

For wall boundary condition, eulerian wall, adiabatic wall, viscous wall and fixed temperature wall are available.

Third order Shu-Osher numerical scheme is used in order to advance the solution from time t^n to time t^{n+1}:

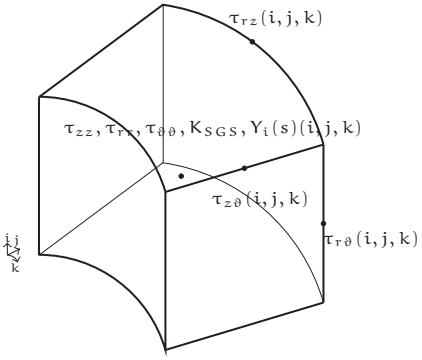

Fig. 4: Viscous Stress Position in a Cell

$$\begin{cases} u^{n+1} = u^n + h\sum_{i=1}^{s} b_i k_i^n & n = 0,..,N-1 \\ u^0 = u(t_0) \end{cases} \tag{15}$$

where

$$\begin{aligned} h &= t^{n+1} - t^n \\ k_i^n &= F\left(t_n + c_i h, \quad u^n + h\sum_{j=1}^{i-1} a_{ij} k_j^n\right) \qquad i = 1,..,s \\ c_1 &= 0 \\ \sum_{j=1}^{0} \cdots &= 0 \end{aligned}$$

ant the coefficient are set to:

$$\begin{aligned} &c_2 = c_3 = 0 \\ &b_1 = b_2 = \tfrac{1}{6}, \quad b_3 = \tfrac{2}{3} \\ &a_{21} = 1, \quad a_{31} = a_{32} = \tfrac{1}{4}. \end{aligned}$$

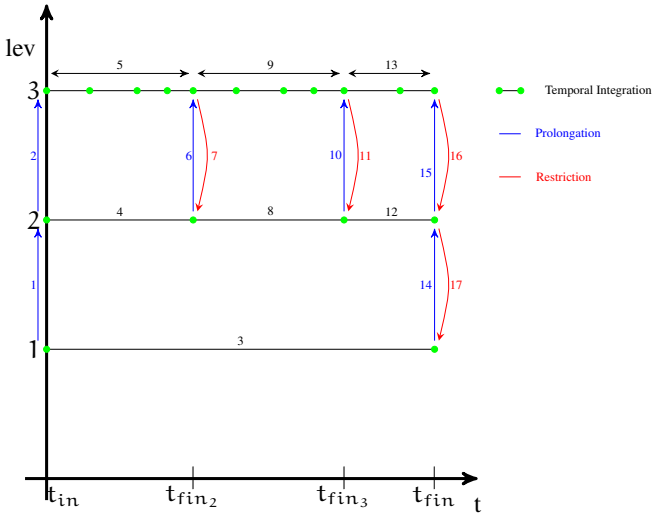

Fig. 5: Time Evolution Algorithm

3. Mesh Refinement

3.1. Multi-Level Approach

Mesh refinement technique developed for HeaRT code was first based on a multi-level approach: a coarse grid is collocated on the entire domain, while in suitable zones (where gradients are bigger) finest level are a-priori generated; mesh refinement has constant ratio=2 for every direction, so a three dimensional coarse cell contains 8 fine cells. Grid levels are properly nested: fine edge grid points have to be included in the coarse grid level, except for boundary condition edges.

In such approach, different grid levels communicate by means of two different operators: restriction and prolongation. First is suitable for communication between fine grid internal points and corresponding coarse points while the latter is used for communication from coarse points to the corresponding fine ghost cells.

Solution algorithm is represented in figure 5: is clear that communications between different grid levels have a fundamental role; with communication at preset intervals, grids are tied each other and the numerical solutions on the different levels are all coherent. For a turbulent flow field, for example, finest grid locates and identifies little vortices and transfers numerical solution to the overlapped coarse grid, that therefore can take into account to the mixing phenomena.

Restriction is implemented by the mean of a sum (weighted by the fine cell volume fraction contained in the corresponding coarse cell, equation 16) over all fine cells contained in the control volume of the coarse variable: due to the staggered formulation adopted in HeaRT code, control volume for scalar variables corresponds to the volume of the grid cell, while for mass fluxes control volume is shared between two neighboring grid cells.

$$\Phi_C = \frac{\sum_{i=1}^{n} \phi_{f_i} V_{f_i}}{\sum_{i=1}^{n} V_{f_i}} \tag{16}$$

Prolongation is implemented by the mean of bilinear or trilinear interpolations: first for fine mass fluxes that are collocated on the same interface of the corresponding coarse mass fluxes, latter for scalars and for fine mass fluxes collocated within the corresponding coarse cell.

3.1.1. Numerical Tests

In order to validate mesh refinement technique early described, numerical simulation of Rankine Vortex on a cylindrical numerical grid is been performed, with two grid levels: the coarse one covers the entire flow field, while

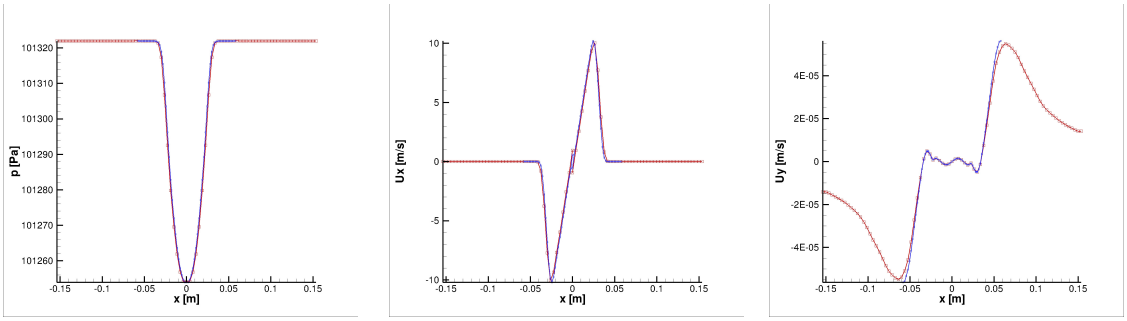

(a) (b) (c)

Fig. 6: Pressure, Tangential and Radial Velocities Flow Fields

the fine one contains the vortex. Numerical results are good, and the presence of a fine grid on vortex boundaries, where gradients are bigger, avoids birth of spurious oscillations (figure 6).

The next step was the simulation of Sommerfeld and Qiu experiment with mesh refinement technique: the computational grid is refined in proximity of the inlet of the test chamber, where the bluff body take place; unfortunately, numerical results aren't good and in the gas phase flow field, after some iterations, spurious pressure oscillations born on the finest level (3) and propagate to the coarsest levels (2 and 1), as can be seen in figure 5.

This behaviour has led to a deeper analysis of the multi-resolution technique and its algorithm implemented in the HeaRT code: in particular, multi-level approach has been abandoned and a new approach, based on joined grids, has been adopted.

3.2. Joined Grids Approach

In the joined-grids approach, numerical grids with different spatial resolution are not overlapped but joined each other: a coarse grid isn't present on the entire computational domain. So the communication between different resolution grids take place only on the ghost cells that are necessary for numerical integration of cell next to grid boundaries.

Anyway is always possible to recognize two different operators for communication from fine to coarse grid and from coarse to fine grid: first is obtained by meant of an accurate and conservative interpolation: fine values are obtained by a Taylor series expansion, where the first and second order derivatives arise from the solution of a system of equations via Least Square method. The choice of interpolation domain isn't simple, because of the staggered formulation adopted: for some fine cell, interpolator is composed only from coarse points that surround simmetrically the coarse centroid of interpolation; in other cases the interpolator is made up by coarse and fine points and the domain is not symmetrical with respect to the coarse centroid.

For communication from fine to coarse grid, the same restriction operator of multi-level approach is used.

This technique is under accurate validation: after some basic monodimensional and bidimensional simple tests, Sommerfeld and Qiu experiment will be simulated again.

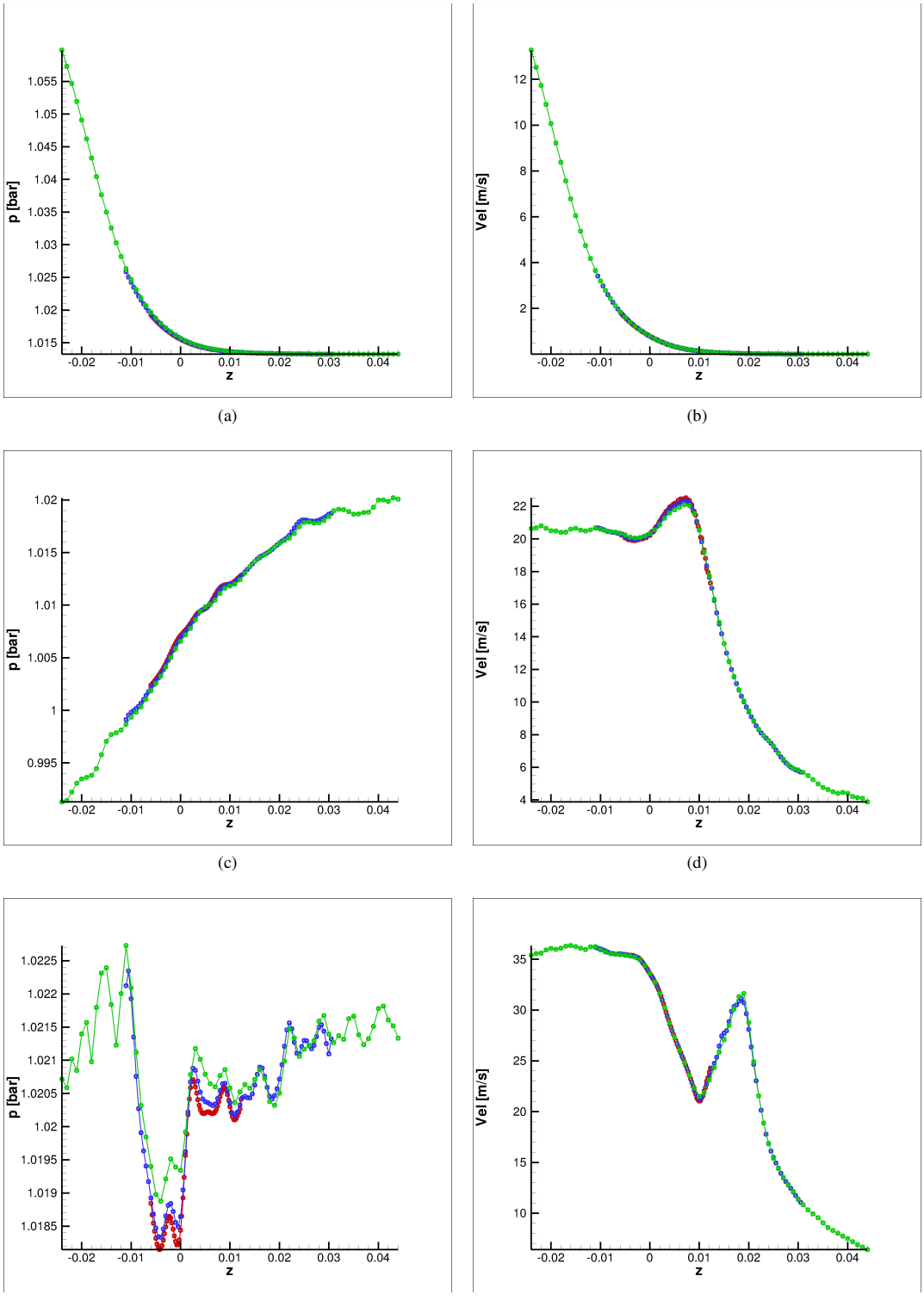

Fig. 7: Pressure and Velocity Magnitude Along z Direction

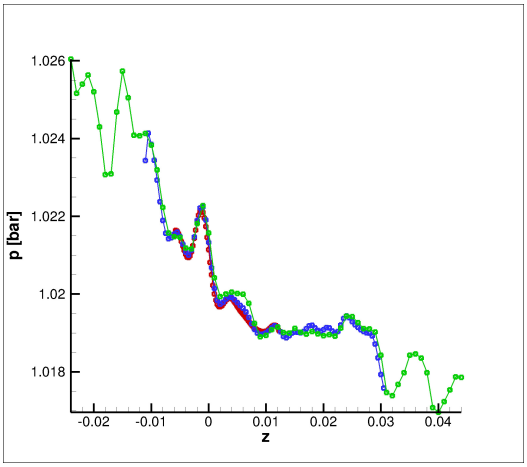

(g)

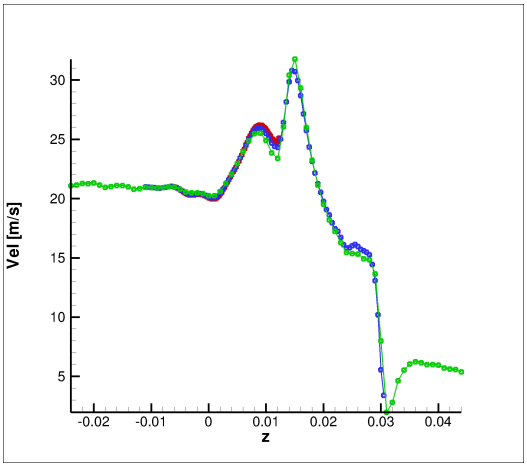

(h)

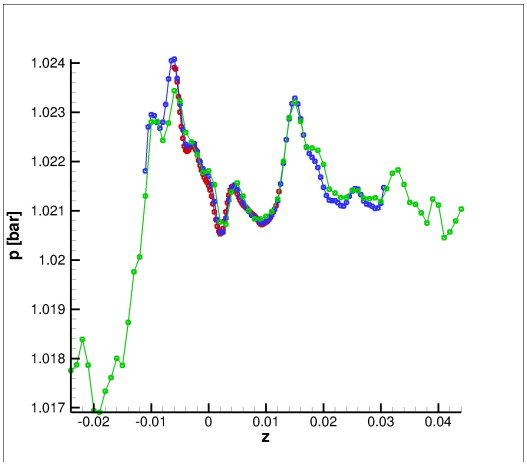

(i)

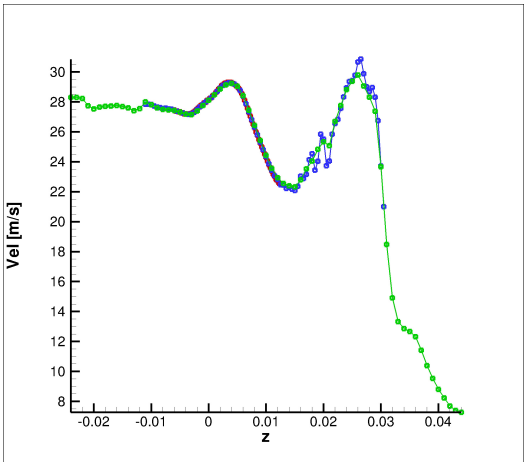

(j)

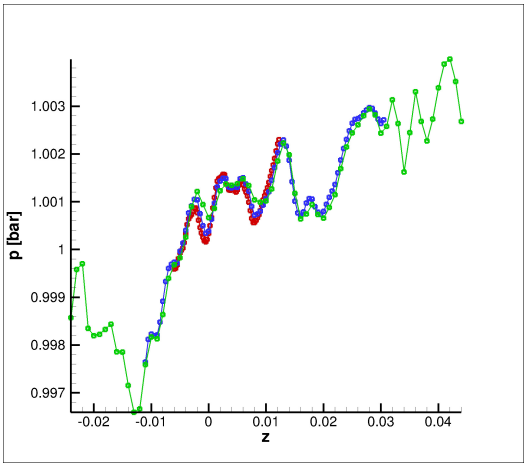

(k)

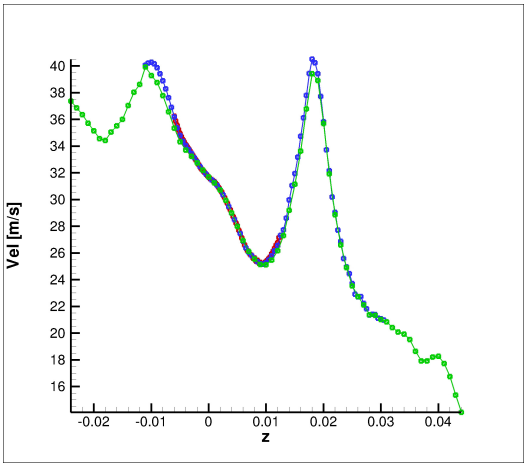

(l)

Fig. 6: Pressure and Velocity Magnitude Along z Direction

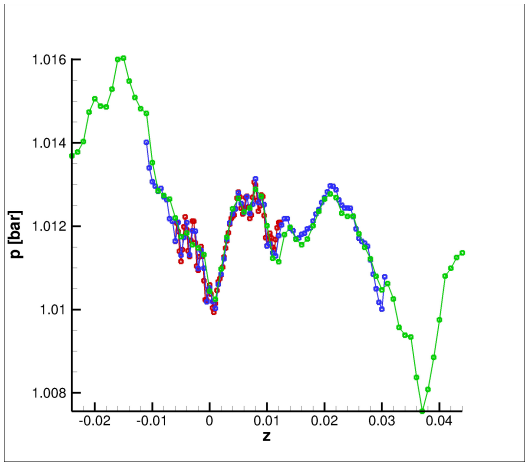

(m)

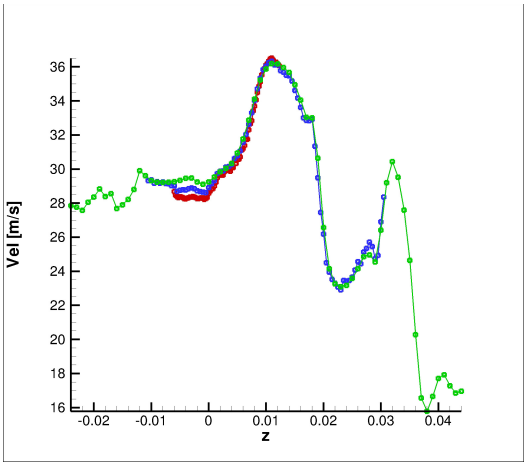

(n)

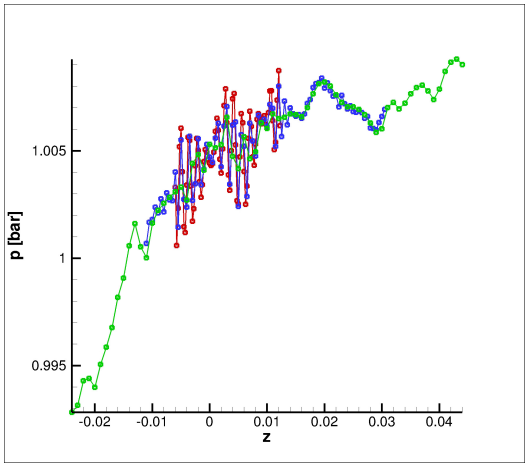

(o)

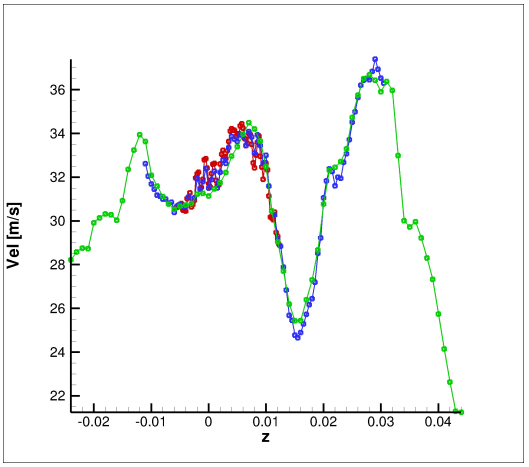

(p)

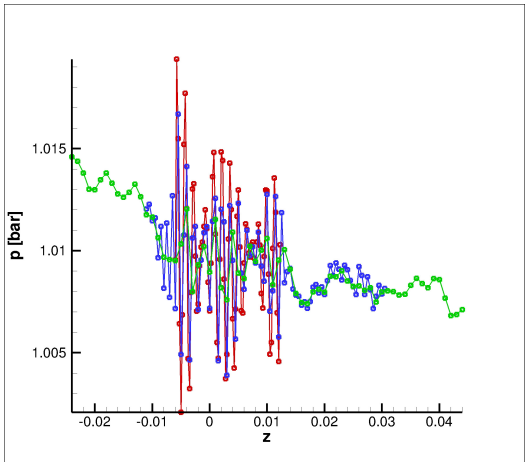

(q)

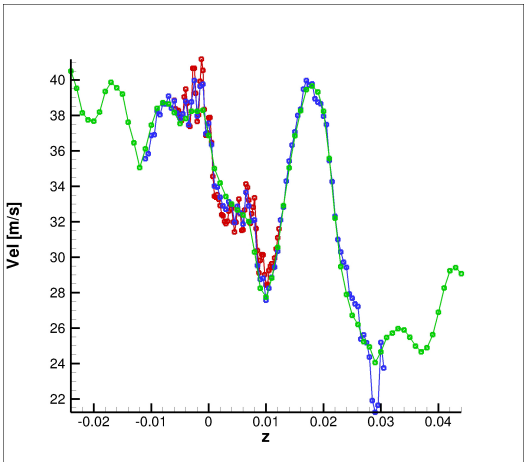

(r)

Fig. 5: Pressure and Velocity Magnitude Along z Direction